Materials Science & Engineering A 763 (2019) 138117

Contents lists available at ScienceDirect

Materials Science & Engineering A

journal homepage: www.elsevier.com/locate/msea

The effect of composition and microstructure on hardness and toughness of Mo_2FeB_2 based cermets

Maxim B. Ivanov[a,*], Tatiana N. Vershinina[b], Victor V. Ivanisenko[b]

[a] S7 R&D Center, Vostochnaya 5, M4 Technopark, Leninskiye Gorki, Moscow Region, 142712, Russia
[b] Belgorod National Research University, Pobedy street 85, Belgorod, 308015, Russia

ARTICLE INFO

Keywords:
Mo_2FeB_2 based cermet
Alloying
Microstructure
Mechanical properties

ABSTRACT

Mo_2FeB_2 based cermets with various Ni, Cr and C concentrations were prepared. The effect of Ni, Cr and C on the phase composition and microstructure was investigated by scanning electron microscopy (SEM), energy dispersive X-ray analysis (EDS) and X-ray diffraction (XRD). Hardness (HRA) and fracture toughness (K_{1c}) were also measured. It was found that nickel alloying leads to formation of two-phase state represented by Mo_2FeB_2 boride and austenite. Chromium alloying results in austenite to ferrite transformation and $M_{23}C_6$ and M_6C carbide precipitation in the case of carbon doping. Also, it was found that chromium influences the borides mean size. Observed changes in the phase composition and microstructure affect the hardness and fracture toughness of investigated materials.

1. Introduction

Reactive liquid phase sintered Mo_2FeB_2 complex boride base cermets have good mechanical properties and excellent corrosion and wear resistance [1,2]. These materials have successfully applied to hot copper extruding dies, injection molding machine parts, etc.

The binder phase in Mo_2FeB_2 base cermets has eutectic composition on the base of iron obtained during liquid phase sintering. Consequently, materials properties are especially sensitive to alloying. For example [3–5], traditional alloying elements for iron alloys such as chromium, manganese and nickel have a strong influence on the mechanical properties of these cermets.

It can be seen from the experimental data that Cr addition can improve the properties of Mo_2FeB_2-based ceramic by grain refinement and solid solution strengthening [6]. It was pointed out in Ref. [7] that the hardness and transverse rupture strength of Mo_2FeB_2-based cermets are improved with the increase of Cr content.

Ni addition improved the properties of Mo_2FeB_2-based cermets though raising the properties of the binder phase [8]. Takagi et al. stated that a maximum of transverse rupture strength was observed for cermets doped by 2.5% Ni [3].

Contradictory data on the influence of carbon on microstructure, phase composition and mechanical properties of cermets are presented in a literature. Yu H. et al. [9]. have found that carbon has a positive influence on the particle size reduction and leads to transformation of ferrite matrix into martensite one. But both transverse rupture strength (TRS) and fracture toughness monotonically decrease with the increase of carbon content. The base composition with 0.5 wt% C has been selected for the investigation of boron concentration influence on cermets properties [10]. According to Ref. [10] a moderate concentration of carbon in an amount of 0.5 wt % is enough for substantial cermets hardness increase.

Takagi [11] suggested that a higher TRS could be obtained when Mo was added to match the Mo/B atomic ratio of 1.0. The third phase such as M_6C (M: metal) is precipitated in the Mo-rich cermets with the Mo/B atomic ratio above 1.0 [11]. It's obvious that M_6C phase precipitation requires carbon presence, so the rest plays a key role in microstructural design of cermets. However, as it was claimed in Ref. [10], new $M_{23}B_6$ type phase was detected in carbon alloyed cermet. On the other hand in steelmaking it is well known that complex carbon and boron alloying of iron leads to the precipitation of a $M_{23}(B,C)_6$-type phase [12]. Thus "newly" founded $M_{23}B_6$-type phase in carbon and chromium alloyed cermet investigated in Ref. [10] is in fact a typical for steel $M_{23}C_6$ carbide with partial substitution of carbon with boron.

Doping concentration of alloying elements plays a crucial role in the achievement of optimal microstructure parameters in the terms of mechanical properties. Unfortunately, there is no reliable data about the influence of chromium and nickel on the properties of high carbon alloyed cermets.

In present work the influence of the phase composition and

* Corresponding author.
E-mail address: m.b.ivanov@s7.ru (M.B. Ivanov).

https://doi.org/10.1016/j.msea.2019.138117
Received 18 March 2019; Received in revised form 4 July 2019; Accepted 5 July 2019
Available online 12 July 2019
0921-5093/

Table 1
Compositions of the Mo_2FeB_2 -based cermets (wt.%).

Alloy	Element							
	Mo	Fe	Cr	Ni	B	C	Si	Other
1	55.0	33.5	2.0	2.0	7.0	–	0.28	0.22
2	55.0	31.5	2.0	4.0	7.0	–	0.28	0.22
3	55.0	31.5	3.0	3.0	7.0	–	0.25	0.25
4	54.7	20.7	_-	16.0	6.3	1.7	0.22	0.38
5	54.7	22.1	2.6	12.0	6.3	1.7	0.28	0.32
6	54.7	23.4	5.2	8.0	6.3	1.7	0.34	0.36
7	54.7	24.7	7.8	4.0	6.3	1.7	0.39	0.41
8	54.7	26.0	10.4	–	6.3	1.7	0.46	0.44

microstructure of Mo_2FeB_2–Fe based cermets on the hardness/fracture toughness relation in dependence of nickel, chromium and carbon alloying were investigated.

2. Material and methods

Table 1 gives the designed compositions of Mo_2FeB_2–Fe cermets with different levels of Cr, Ni and C content. Investigation of Ni and Cr alloying influence on the microstructure, phase composition and mechanical properties were conducted using alloys 1, 2 and 3 with 7,0 wt % B listed in Table 1.

Commercial powders of nickel (2 μm), chromium (40 μm) and molybdenum (3 μm) were used as a raw material. Ball-milled powder of ferroboron were used as a source of iron and boron for alloys listed above. Similar studies of the effect of chromium and nickel content on microstructure and mechanical properties of carbon added alloys (6,3 wt % B and 1,7 wt % C) were carried out using alloys 4–8 given in Table 1. The powder mixtures prepared from ferromolybdenum, ferrochromium, pure Ni and B_4C (chemical composition corresponds to national Russian standards) were ball-milled in a planetary mill Pulverisette 5 in benzine for 1 h. These alloys characterized by presence of copper, phosphorous and sulfur (impurities of raw components) with the total concertation pointed in Table 1 as “Others”.

Green compacts with Ø22 mm and height of 8 mm were produced by axial pressing at 100 MPa. Compacted samples were sintered in vacuum 10^{-4} torr. The influence of sintering temperature (1393, 1413, 1433 and 1473 K) on the microstructure and mechanical properties was investigated for alloy 3.

For metallographic examination samples were prepared by a two-step polishing procedure using a rotary polishing machine LaboPol-5 (Struers): first grinding with silicon carbide paper, then grinding with diamond suspension on a polishing cloth.

SEM investigations (back scattered mode) were carried out in Quanta 600 FEG equipped with system for energy dispersive spectrometry (EDS).

ARL X'TRA diffractometer with CuK_α radiation was used for XRD measurement at Bragg-Brentano focusing mode. The diffraction lines were recorded for 2θ = 20–100°with a step of 0.01°. Quantitative phase analysis was performed using the program PowderCell 2.4.

The hardness HRA of sintered samples was measured using a standard Rockwell hardness measuring device (600 MRD Instron Wolpert Wilson Instruments) with a load of 60 kgf.

The Palmqvist method [13] was used to determine the fracture toughness of investigated materials. A 1 mm distance between indentations was kept in order to avoid overlapping effects. Indentation load was 60 kgf. Lengths of cracks were measured by light optical microscopy (Olympus GX71).

Contiguity was measured in two dimensions by quantitative analysis of SEM images based on the number of intercepts per unite length of test line N.

$C_{ss} = 2N_{SS}/(2N_{SS} + N_{SL})$.

N_{SS} denotes a number of solid-solid intercepts, N_{SL} denotes solid-binder (liquid) intercepts [14].

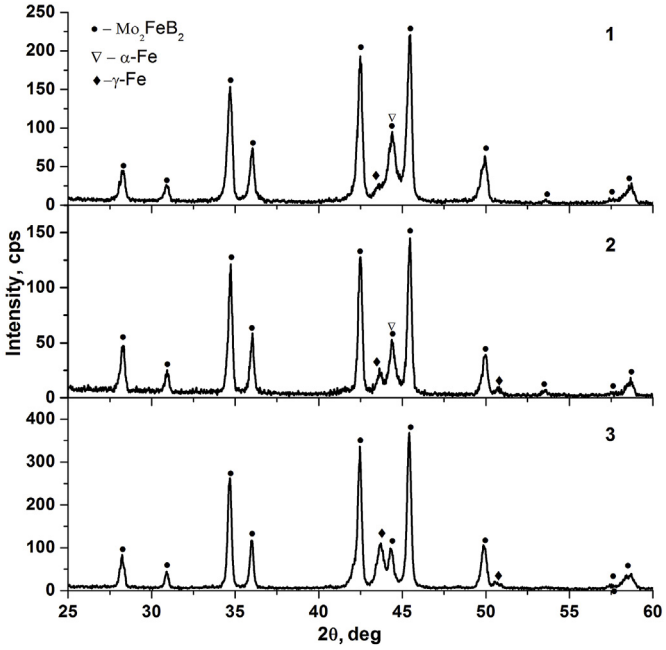

Fig. 1. XRD patterns of Mo_2FeB_2 based cermets: 1 – alloy 1; 2 – alloy 2; 3- alloy 3.

3. Results

Fig. 1 shows XRD patterns and Fig. 2 shows the microstructure of carbon free cermets (7,0 wt % B) with various Cr and Ni contents. All investigated cermets contain Mo_2FeB_2 hard phase and the ferrous binder phase. As far as chromium has ferrite stabilizing effect, and nickel is an austenite stabilizer, the binder phase is presented by α-Fe and γ-Fe (Table 2). The increase of the nickel concentration leads to the increase of the fraction of austenite in a binder. The binder contains ferrite and austenite in alloys 1 and 2. The alloy 3 is characterized by austenite only binder phase.

Fig. 3 shows a comparison of hardness and fracture toughness of sintered carbon free alloys (7,0 wt % B). As can be seen, the highest value of fracture toughness corresponds to the cermet 2, wherein the binder is fully represented by austenite and microstructure is characterized by the presence of hard particle-free “islets".

The investigation of the influence of the annealing temperature on the microstructure of hard alloys of Mo_2FeB_2–Fe system was performed on alloy 3. Heterogeneous structure formed during annealing at 1393 K through 10 min (Fig. 4a). Boride particles are distributed non-uniformly in a volume and “islets” of metallic phase are observed. The gradual temperature increase to 1433 K leads to reduction of “islets” (Fig. 4 b-c) sizes and finally to their vanishing at 1473 K (Fig. 4d). The growth of mean size of Mo_2FeB_2 crystals also is observed during annealing. There is a nonlinear dependence between boride crystal size and annealing temperature (Table 3), which was also observed in Ref. [15].

The increase of the annealing temperature leads to the decrease of the contiguity ratio (Table 3). Consequently, it means a reduction of quantity of solid/solid contacts and indicates a growth of volume fraction of borides completely surrounded by the binder phase. A wetting of hard particles by tough phase influences on properties of material because it facilitates the formation of stable structure and reduction of structural stresses in material as a result [16].

A microstructure changes caused by annealing significantly affect the fracture toughness of cermets. (Fig. 3). The fracture toughness of cermets increases with a temperature growth from 1393 to 1433 K. This may be due to the increase of the borides size and the thickness of metal

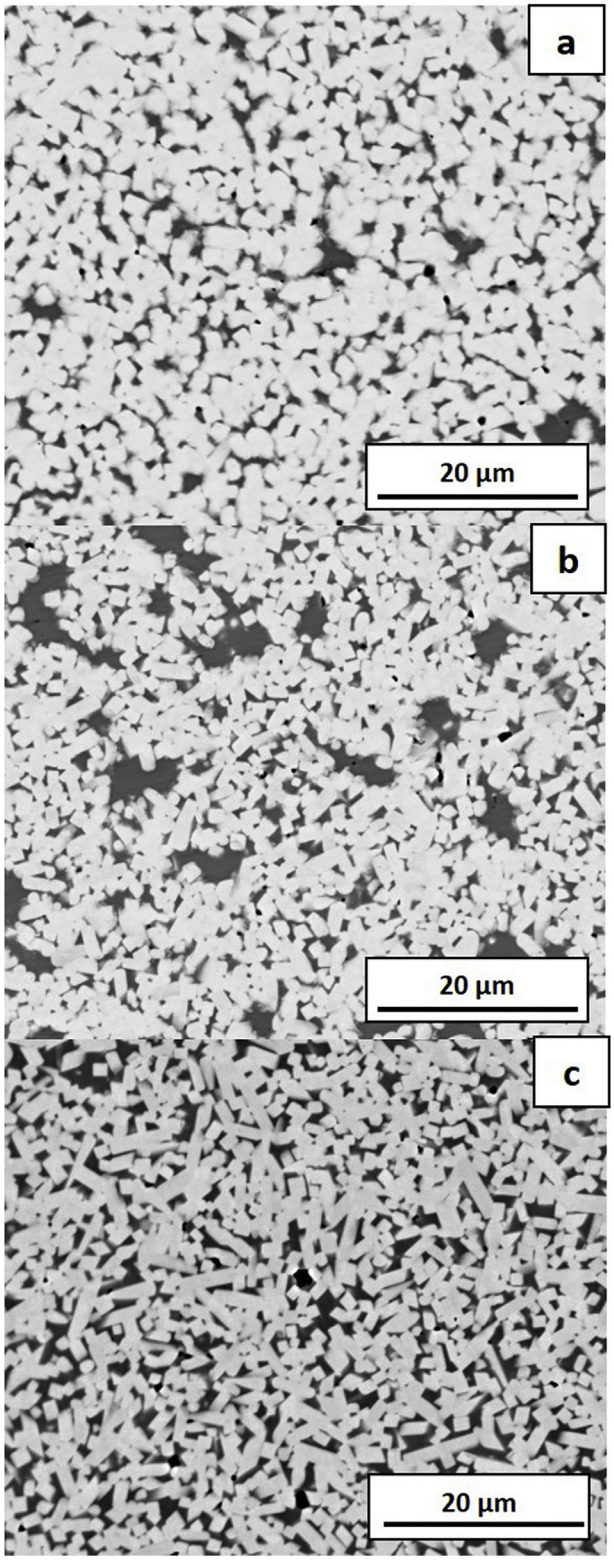

Fig. 2. Microstructure images of cermets (a) 1; (b) 2; (c) 3.

interlayers. However, the fracture toughness decreases sharply after annealing at 1473 K, the reason of the above will be discussed further.

The ratio of chromium and nickel has a similar effect on the phase composition of the binder phase in materials additionally doped with carbon. In the case of nickel doping binder was represented by austenite. Chromium introduction and its concentration increase leads to the decrease of austenite volume fraction. Substitution of nickel by

Table 2
Phase composition of cermets (XRD).

Alloy	Mo_2FeB_2	γ-Fe	α-Fe	M_6C	$M_{23}C_6$
1	78 ± 2	2 ± 2	20 ± 2	–	-
2	83 ± 2	7 ± 2	10 ± 2	–	-
3	88 ± 2	–	12 ± 2	–	-
4	77 ± 2	23 ± 2	–	–	–
5	77 ± 2	15 ± 2	–	3 ± 2	5 ± 2
6	80 ± 2	11 ± 2	–	4 ± 2	5 ± 2
7	80 ± 2	8 ± 2	–	5 ± 2	7 ± 2
8	74 ± 2	–	8 ± 2	8 ± 2	10 ± 2

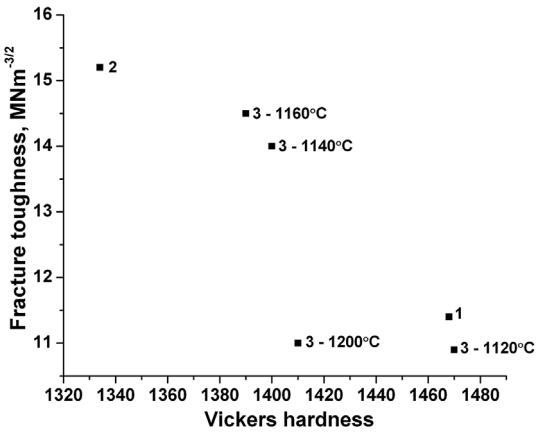

Fig. 3. Fracture toughness vs hardness for cermets alloyed by Ni and Cr.

chromium leads to full γ→ α transformation (Table 2). This is since chromium has ferrite stabilizing effect. It should be mentioned that volume fraction of the binder is decreased with the chromium concentration increase.

The investigation of microstructure (Fig. 5) and phase composition (Fig. 6) of sintered samples reveals that nickel and chromium alloying affected the phase composition of secondary phases else. The chromium doping leads to the $M_{23}C_6$ and M_6C carbides precipitation. The chromium concentration increase is resulted in the increase of volume fraction of $M_{23}C_6$ carbide (Table 2).

According to EDX data M_6C carbide is presented in two types: $(Mo,Fe)_6C$ and Ni_3Mo_3C. The last one is characterized by high silicon content (Fig. 7). The volume fraction of Ni_3Mo_3C carbide decreases with the increase of nickel concentration. The volume fraction of this carbide is the highest in the cermet 8 (~5 vol %) and the lowest in the cermet 5 (~1 vol %).

It was found that silicon is dissolved in a binder in the cermet 5. Also, according to EDX it is homogeneously spreads in austenite in the state which is contains no chromium.

Chromium and nickel alloying affects the mean size of boride crystals (Fig. 5, Table 4). The decrease of the nickel concentration and the simultaneous increase of chromium concentration lead to the reduction of mean size and change in morphology of boride crystals. The shape of borides changes from clear quadrangular to somewhat with rounded angles. It can be attributed to the decrease of anisotropy of the surface free energy of different crystallographic planes of Mo_2FeB_2 crystals due to substitution of Mo atoms by Cr atoms [8]. Also, it can be noted that bright internal area is visible in a boride in the state with higher chromium content (Fig. 5 c-e). It can be resumed that the periphery of borides is presented by $(Mo,Cr,Fe)_3B_2$ phase and a central part is presented by Mo_2FeB_2 one. Some changes of lattice parameters also indicate the substitution of Mo atoms by Cr atoms (Fig. 8).

As it can be seen from Fig. 9 the chromium concentration increases and the nickel content decreases in carbon doped cermets lead to the increase of material hardness HV_{60}, which is in correlation with the

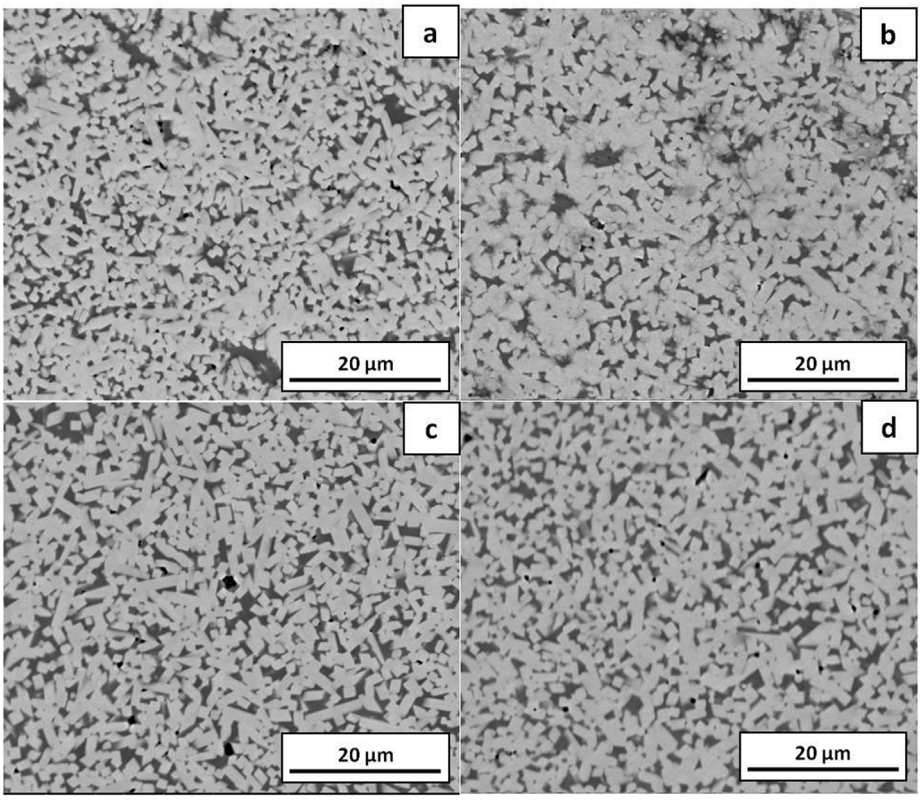

Fig. 4. Microstructure images of cermet 3 annealed at: (a) 1393 K; (b) 1413 K; (c) 1433 K; (d) 1473 K.

Table 3
Effect of annealing temperature on a contiguity ratio and mean crystal size in cermet 3.

Annealing temperature, K	Contiguity ratio	Mean crystal size, μm
1393	0,42 ± 0.02	1.5 ± 0.2
1413	0,33 ± 0.02	1.5 ± 0.2
1433	0,31 ± 0.02	1.9 ± 0.2
1473	0,23 ± 0.02	2.1 ± 0.2

increase of the total volume fraction of hard phases presented by borides and carbides (Table 2). Meanwhile hardness is affected by the crystal size reduction (Table 4). The fracture toughness has a typical opposite dependence and sharply decreases with the increase of the hardness (Fig. 9).

4. Discussion

We can suggest that both $M_{23}C_6$ and M_6C types of carbides can precipitate in Mo_2FeB_2-based cermet alloyed with carbon. The definite phase composition depends on carbon concentration, on the presence of other alloying elements like chromium and silicon, and on the binder state (e.g. it is austenitic or ferritic one). This statement is in well agreement with the data obtained in Refs. [10,11].

The higher volume fraction of M_6C carbide in cermet with the higher chromium content is associated with two factors. Firstly, the small nickel and the high chromium concentration lead to the decrease of the austenite volume fraction which is characterized by higher carbon solubility in comparison with ferrite [17]. Since carbon does not dissolve in ferrite, it tends to form carbides. Secondly, the reason of M_6C carbide precipitation is the presence of silicon which is introduced into the alloys with ferrochromium as an impurity, that is the chromium concentration increase is accompanied by the higher silicon content. As far as silicon is a stabilizer of Ni_3Mo_3C type phase, precipitation of this carbide is typical for nickel heat resistant alloys. The literature has no data about location of atoms in lattice sites of such carbides. There are several formulas which describe composition of Ni_3Mo_3C carbide: $(Ni,Si,Fe)_3(Mo,Cr)_3C$ [18], $(Ni,Si,Cr)_3Mo_3C$ [19], $Ni_3(Mo,Cr)_3(C,Si)$ и $Ni_2(Mo,Cr)_4(C,Si)$ [20]. But it can be noted that according to these formulas chromium is incorporated in composition of M_6C carbide too, which is not proven in present work.

The high volume fraction of carbides in Mo_2FeB_2-based cermets alloyed by carbon leads to the high hardness of the materials. However, despite the fact of high boron (6,3 wt %) and carbon (1,7 wt %) content the absence of chromium dramatically mitigates the hardness of cermet with the austenitic binder only.

It can be noted that the toughness and the hardness of cermets with various substitutions of iron by nickel and chromium are mainly determined by the phase composition of the binder, e.g. by the presence and the volume fraction of austenite. Thus, the minor alloyed with Ni and Cr cermet 1 shows the highest hardness, while more alloyed ones (alloys 2 and 3) are sufficiently tougher.

The hardness of investigated materials is more dependent on doping with chromium rather than nickel. Cermet with additional Cr content (alloy 3) is harder than the other one with Ni (alloy 2) while preserving the same total alloying level and the same binder phase composition (austenite). This fact can be attributed both to the strong strengthening effect of Cr on the hardness of ternary boride Mo_2FeB_2 [2] and any austenitic steel (which is playing here the role of the metal binder phase).

Analogous regularity is observed for cermets with carbon alloying. The volume fraction of the binder in both 7 and 8 alloys is 8% and it is fully represented by austenite in alloy 7 and by ferrite in alloy 8. As it can be seen from Fig. 9 this difference caused lower fracture toughness for the latter alloy in comparison with the first one.

It should be noted the difference in the arrangement of borides particles in the binder phase. The “islets” (or “liquid-filled lakes” [16]) of binder phase are observed in cermet 1. Their formation is a

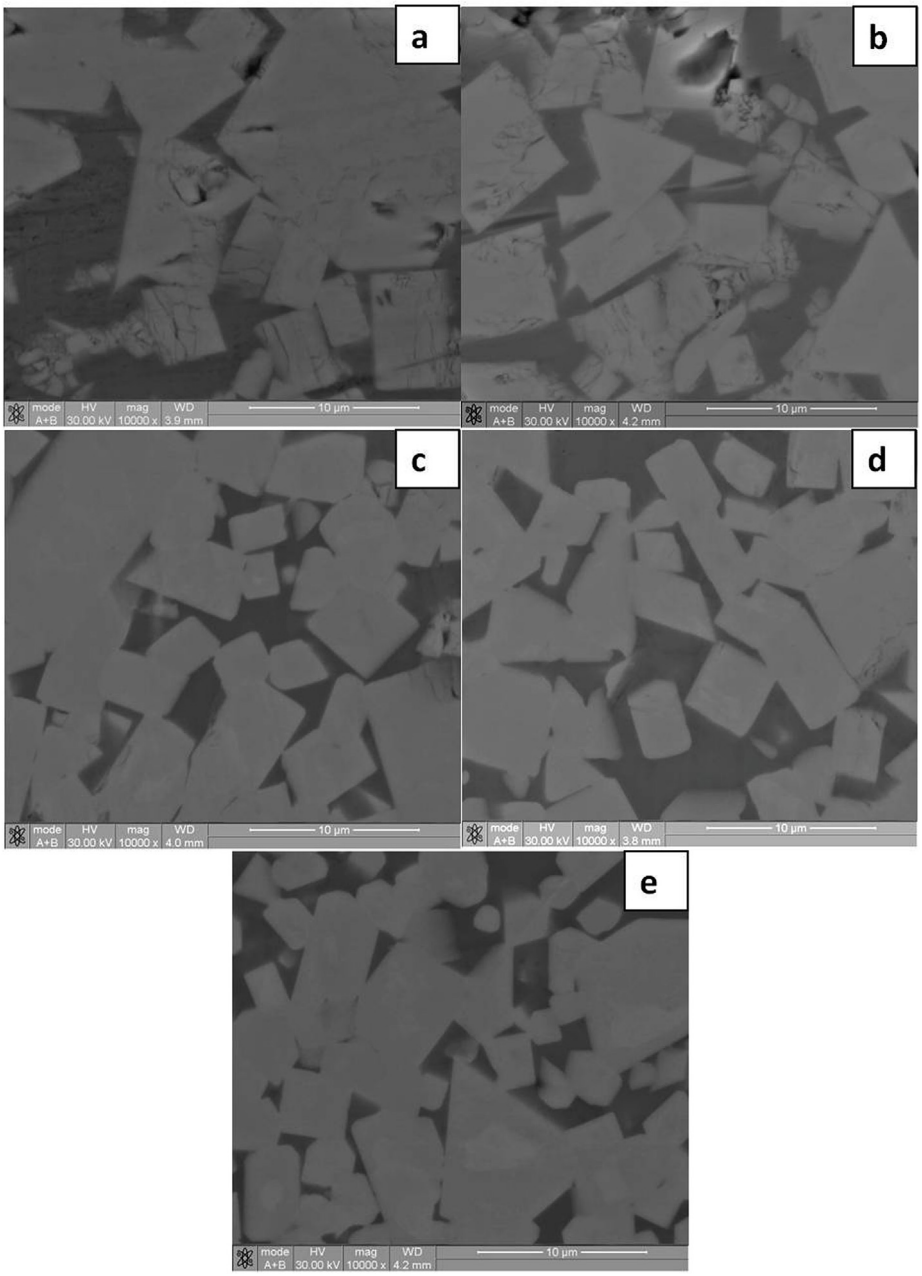

Fig. 5. SEM images of Mo_2FeB_2–Fe cermet microstructure: a – alloy 4, b - alloy 5, c - alloy 6, d - alloy 7, e − alloy 8.

consequence of filling of large pores by liquid when the ratio of the grain size G to pore size d_p satisfies the condition [16].

$$D/d_p = \gamma_{SS}/(2\gamma_{SL}) = \cos(\phi/2) \quad (1)$$

where γ_{SS} – solid-solid grain boundary energy, γ_{SL} - solid-liquid grain surface energy, ϕ – dihedral angle. As can be seen from Table 4, an increase of nickel concentration leads to a decrease of borides mean size with an increase of "islets" size (Fig. 2). According to expression (1), it can be concluded that an increase of nickel concentration at the same chromium concentration leads to an increase of ϕ angle. That is, nickel deteriorates the wettability of the borides surface by liquid.

As it can be seen from the data presented in Tables 1 and 2, the state 3 is characterized by the smallest volume fraction of the binder in comparison with alloys 1 and 2. At the same time, the estimation of the a contiguity ratio (Table 3) shows that the number of solid particle/liquid boundaries increases despite the decrease of volume fraction of the liquid phase during sintering. This behavior of the material can be explained in terms of solid-liquid grain surface energy γ_{SL}. As it is known from the literature [16] small changes of γ_{SL} are enough to give liquid penetration of grain boundaries. For example, a $\phi = 30^\circ$ requires only a 7% decrease in the γ_{SL} to enable grain boundary penetration. In case of the alloy 3, doping with chromium leads to a decrease of γ_{SL} in the materials studied.

It is known that γ_{SL} variation affects the shape of the particles of the solid phase [21]. Particle morphology changes according to the ratio $\beta = \gamma_{hkl}/\gamma_{SL}$, where γ_{hkl} is an interfacial energy per unit area of the {hkl} planes. β increase cause shape-change of solid particles from sharp-edge to rounded-edge. In Ref. [8] change of Mo_2FeB_2 borides shape was explained by γ_{hkl} increase due to an increase in chromium concentration in borides. Let us compare the microstructure and phase composition of cermets, additionally doped with carbon. For example, particles of Mo_2FeB_2 borides in alloy 4 have sharp-edge shape. At the same time binder phase in this state is austenite, whose stabilization at low temperatures is directly related to the increase of nickel

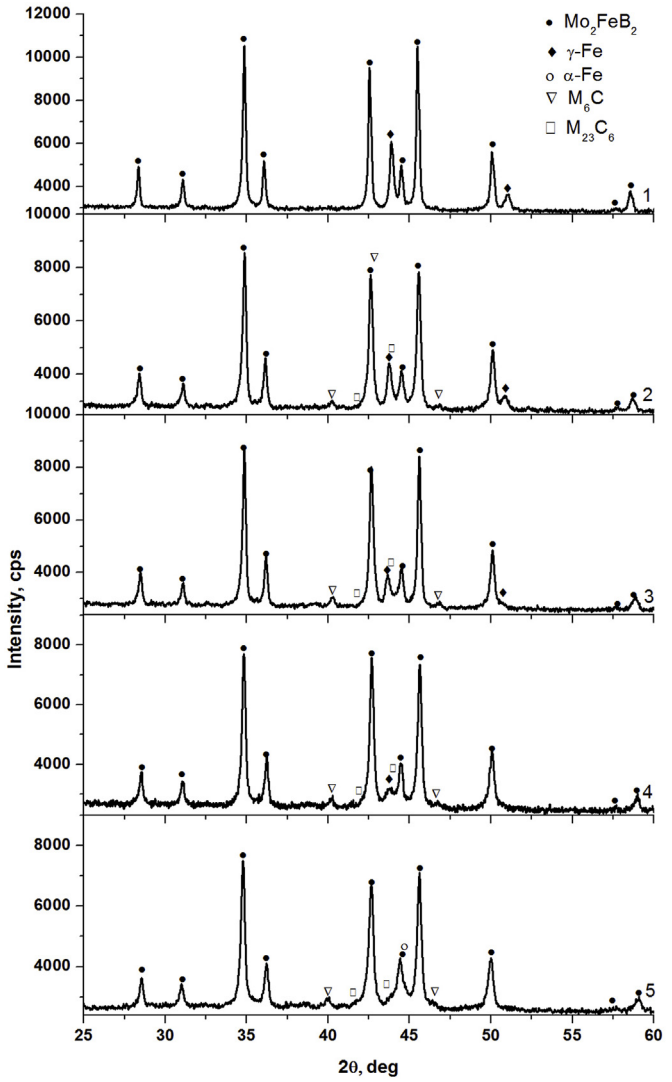

Fig. 6. X-ray diffraction patterns of Mo_2FeB_2–Fe cermets: 1 – alloy 4, 2 – alloy 5, 3 – alloy 6, 4 – alloy 7, 5 – alloy 8.

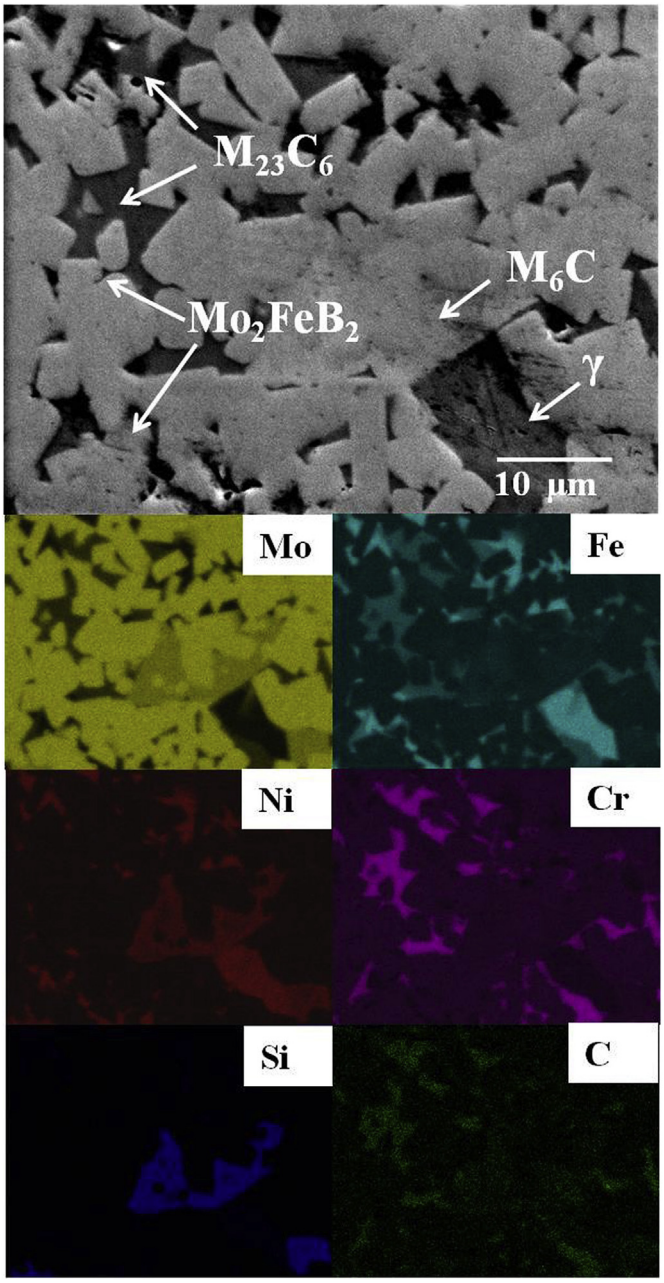

Fig. 7. High resolution EDS mapping of the alloy 7.

Table 4
Mean crystal size of Mo_2FeB_2 borides.

Alloy	Mean crystal size, μm
1	1.5 ± 0.2
2	1.3 ± 0.2
3	1.3 ± 0.2
4	4.9 ± 0.3
5	4.7 ± 0.3
6	4.3 ± 0.3
7	4.1 ± 0.3
8	3.4 ± 0.3

concentration. The binder phase in alloy 8 is fully represented by chromium stabilized ferrite. Thus, decrease of γ_{SL} which is associated with a decrease in nickel concentration and an increase in chromium concentration in the liquid during sintering facilitates to shape-change of borides from sharp-edge to rounded-edge too.

It is well established for tungsten carbide based hard alloys [22,23] that hardness is inversely related to fracture toughness with varying of the grain size and the volume fraction of the binder phase, but with a constant phase composition of the carbide core. This statement extends down to the nanometer size of the particles of the hard phase [24], as well as for the case of dispersion hardening of a cobalt binder [25]. In the last revision work [26] a linear relationship was established between mean free path (MFP) and fracture toughness.

However, there are opposite data for cermets on a tungsten-free base (namely, Ti(C,N)-based). So, it was shown in already classic work [27] that ultrafine grained cermet on the base of TiC and nickel-molybdenum binder is much harder, but at the same time it is somewhat tougher than a fine-grained analog.

In Ref. [28] a completely similar result was obtained for a case of addition of coarse particles of titanium carbonitride to a finely grounded mixture: hardness and crack resistance reduced at the same time. The work is notable because the investigation was conducted not only for two types of cermets with coarse and fine grains, but the functional dependence of mechanical properties on the grain size was built. However, it should be considered that two powders with different particle size were used in experiments, and the average grain size of the cermet was controlled by varying of the volume fraction of each

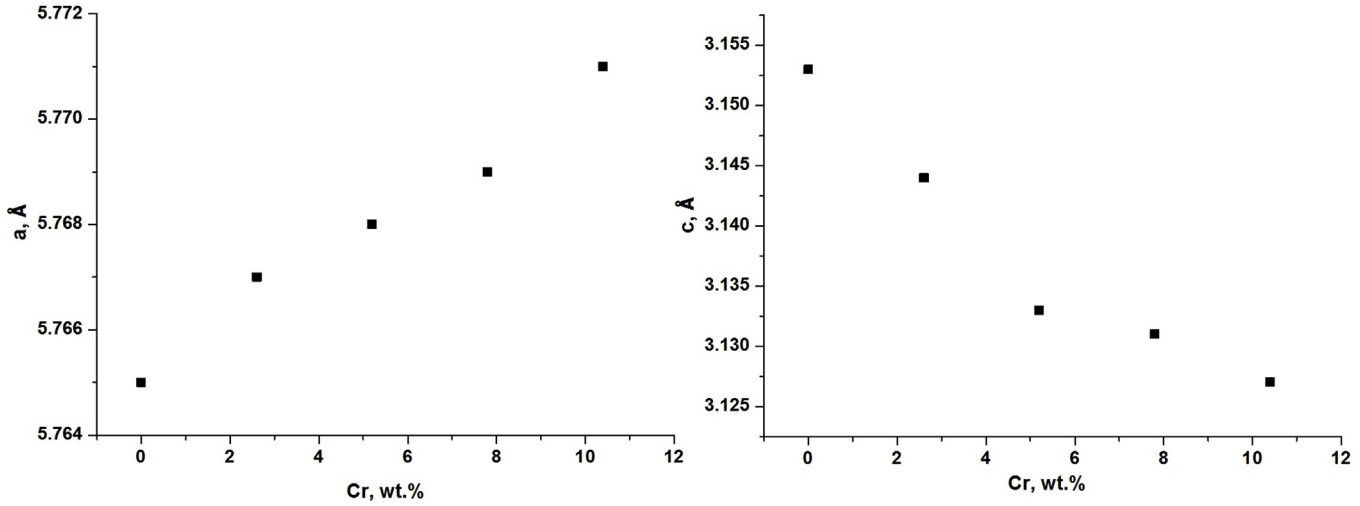

Fig. 8. The dependence of lattice parameters of Mo_2FeB_2 borides on Cr content for cermets alloyed by carbon.

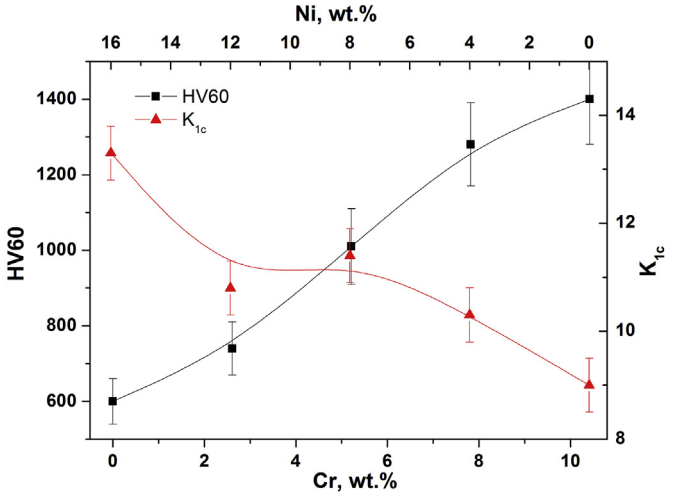

Fig. 9. The dependence of hardness and fracture toughness of Mo_2FeB_2–Fe cermets on nickel and chromium content.

powder. The authors also noted the abnormal grain growth during a sintering process, which could affect the results of the experiments.

The results described above point out the fact that cermets are characterized by an increase of fracture toughness with grain size decrease, as opposed to hard alloys based on tungsten carbide.

However, it was shown in Ref. [29] that a grain size decrease in a cermet with a nickel binder leads to a moderate grain-boundary strengthening, while the fracture toughness decreases. A similar result was obtained in Ref. [30]. It is confirmed the principle that the higher is the hardness the lower is the fracture toughness. This is obtained by comparing mechanical properties of cermets with hard phase crystals of micron and submicron size. Thus, there is a contradiction both in the interpretation and in the primary data of different papers.

Recent studies of cermets [31–33], in which tungsten carbide is not the main reinforcing phase, have shown that under the condition of natural brittleness of the hard phase (Ti, Me)(C, N) an increase of fracture toughness is achieved in the case of solid-solution alloying and core-rim structures of the carbo-nitrides. Changes of physical and chemical properties of the hard phase and the interfaces result in the transition from transgranular to intergranular fracture accompanied by crack deflection.

However, it was stated in Ref. [34] that elastoplastic properties of the hard phase are more important for fracture toughness than a presence of a core-rim structure. In Ref. [35] it has also been shown that a transition to a single rim-phase structure of Ti(C,N) hard phase considerably increases fracture toughness of the material.

Thus, the nature of the fracture toughness dependence on the grain size is inherently associated with the state of interfaces (phase and elemental composition) and elastoplastic properties of the hard phase. If the latter changes, for example, during the grinding process before sintering, then a discussion on the physical causes of the effect of grain size on a fracture toughness is not objective.

In the present work it is shown that the hardness naturally decreases with an increase of the borides size (which is associated with an increase of the MFP in the binder), but at the same time the fracture toughness increases. As mentioned above this happens due to the blunting of the crack tip in conjunction with a large MFP, and it is also ensured by the inability of the crack to move in the borides body. It is obvious that the highest values of fracture toughness of cermets based on titanium carbonitride are consistently associated with the additional development of crack bridging. The reason is an anticipated brittle fracture of particles of the hard phase (for example with a core-rim structure), as indicated by a detailed analysis of the results of the articles [31–35]. Probably, for the cermets investigated in the present work the elastic field at the tip of a propagating crack leads to a kind of “delamination” of the boride skeleton — the destruction of the grain boundaries between the neighboring borides that are not wetted by the binder. Secondary cracks are formed, resulting in crack bridging, the main crack branching and stress relief (Fig. 10). The stress relief depends on the size of the plastic deformation zone. The estimation of the value of the plastic deformation zone can be made according to the Irwin equation [36]:

$$r = K/(2\pi\sigma_{0,2}^2)$$

where r –size of the plastic zone, K – fracture toughness, $\sigma_{0,2}$ = 200 MPa – yield stress for typical austenitic steel. The evaluation shows that size of plastic zone r is more than 8 μm (assuming K_{1c} = 14 MPa·$m^{1/2}$) for the cermets under investigation.

As it can be seen, evaluated value of plastic zone size is noticeably higher than the thickness of metal binder interlayer (MFP) in the states after annealing at 1413 and 1433 K. Thus, separation into some small cracks leads to the stress relief and preserves the crack propagation (Fig. 10).

The actual experimentally observed stress relief cannot be described by plastic deformation of the matrix between borides. It covers an area with dimensions in the tens of grains, which inevitably should result in multiple destruction of the grain boundaries between borides crystals (“boride sceleton”) if any.

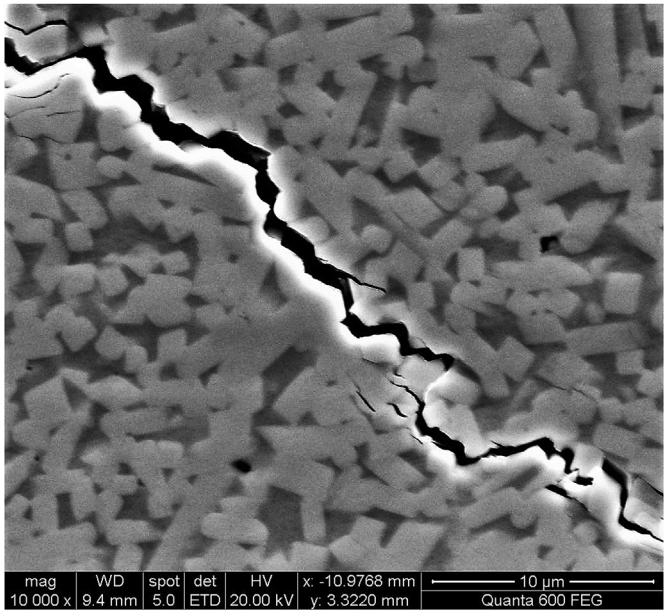

Fig. 10. SEM image of crack formed by Vickers indenter under 60 kgf load.

The complete wetting of boride particles with an iron-based melt for the cermets studied in the present work is realized only at the highest annealing temperature. Therefore, a sudden decrease of the fracture toughness of cermets annealed at the high temperature (1473 K) is most likely realized due to a change in the contiguity ratio (Table 3). A decrease of the contiguity ratio with an increase of the annealing temperature indicates an increase of the fraction of completely wetted boundaries [37,38]. It is known that the transition from incomplete to complete wetting can proceed with increasing temperature, and that it is a true surface phase transformation [39]. In this case of complete wetting $\gamma_{GB} > 2\gamma_{SL}$. Probably, an area of the solid-solid surfaces decreases in the alloy 3 because of realization of this surface phase transformation during increase of annealing temperature. The absence of the brittle grain boundaries of neighboring borides reduces the probability of crack branching and leads to a simultaneous decrease in both the hardness and the fracture toughness of the cermet annealed at 1473 K.

5. Conclusions

Nickel and chromium alloying affect the phase composition of binder phases of Mo_2FeB_2–Fe hard alloys. Nickel doping leads to formation of austenite as binder phase. Chromium introduction leads to $\gamma \rightarrow \alpha$ transformation.

It is shown that doping with chromium and nickel affects the wettability of particles of borides Mo_2FeB_2 by liquid during sintering due to a change of the surface energy of the liquid-solid phase boundary γ_{SL}. Alloying of Mo_2FeB_2-based cermets with nickel increases and with chromium decreases the surface energy of the liquid-solid phase boundary.

The toughness of investigated Mo_2FeB_2-based cermets are mainly determined by volume fraction of austenite and ferrite. The propagation of cracks is also affected by the homogeneity of the borides' distribution in a volume of the material.

The hardness of investigated materials is more dependent on doping with chromium rather than nickel. In the case of hard alloys doped only by chromium and nickel it is associated with solid solution hardening of binder phase and growth of borides hardness. In the case of cermets additionally alloyed by carbon it is first of all related to decrease of the borides size and carbides precipitation.

M_6C phase stabilized by molybdenum can be formed in equilibrium with both austenitic and ferritic binder in cermets alloyed by carbon. Silicon also plays a significant role in stabilization of this phase. A prerequisite for $M_{23}C_6$ carbide precipitation in Mo_2FeB_2-based cermet alloyed by carbon is the chromium content. Consequently, volume fraction of two types of carbides $M_{23}C_6$ and M_6C depends on the degree of supersaturation of the binder phase by carbon. Carbon can be fully dissolved in austenite phase in case of the absence of chromium and silicon in the alloy composition.

Acknowledgements

This work was supported by the Ministry of Science and Higher Education of the Russian Federation in the framework of the state task №11.6894.2017/BCh.

References

[1] M. Komai, K. Takagi, T. Watanabe, Y. Kondo, Effects of cobalt on the properties and phase formation of Mo_2FeB_2 complex boride base hard alloys, AIP Conference Proceedings 231 (1) (1991) 578–583 https://doi.org/10.1063/1.40790.
[2] K. Takagi, Sh Ozaki, M. Komai, S. Matsuo, Sintering mechanism and physical properties of Mo_2FeB_2 type complex boride, Adv. Mater. 93 (1994), https://doi.org/10.1016/B978-0-444-81991-8.50120-5.
[3] K. Takagi, M. Komai, T. Ide, T. Watanabe, Y. Kondo, Effect of Ni on the mechanical properties of Fe, Mo boride hard alloys, Int. J. Powder Metall. 23 (1987) 157–161.
[4] K. Takagi, M. Komai, T. Ide, T. Watanabe, Y. Kondo, Effects of Mo and Cr contents on the properties and phase formation of iron molybdenum boride base hard alloys, Int. J. Powder Metall. 19 (1988) 30.
[5] H. Yu, Y. Zheng, W. Liu, J. Zheng, W. Xiong, Effect of Mn content on the microstructure and mechanical properties of Mo_2FeB_2 based cermets, Int J Refract Met Hard Mater 28 (2010) 286–290 https://doi.org/10.1016/j.ijrmhm.2009.11.001.
[6] F. Yang, Y. Wu, J. Han, J. Meng, Microstructure, mechanical and tribological properties of Mo_2FeB_2 based cermets with Mn addition, J. Alloy. Comp. 665 (2016) 373–380 https://doi.org/10.1016/j.jallcom.2016.01.053.
[7] B. Hu, Y.J. Pan, Q.F. Wang, H. Zhou, Influence of addition element Cr and V on microstructure and properties of Mo_2FeB_2 based cermet, Heat Treat. Met. 36 (2011) 29–32.
[8] Q. Wang, Y. Pan, B. Hu, L. Zhou, Effects of alloys on microstructure and properties of Mo2FeB2-based cermets, Adv. Mater. Res. 399–401 (2012) 399–402 https://doi.org/10.4028/www.scientific.net/AMR.399-401.399.
[9] H. Yu, W. Liu, Y. Zheng, Effect of carbon content on the microstructure and mechanical properties of Mo_2FeB_2 based cermets, Int. J. Refract. Metals Hard Mater. 29 (2011) 724–728 https://doi.org/10.1016/j.ijrmhm.2011.06.001.
[10] H. Yu, Y. Zheng, W. Liu, X. Pang, J. Zheng, W. Xiong, Effect of Mo/B atomic ratio on the microstructure and mechanical properties of Mo_2FeB_2 based cermets, Int. J. Refract. Metals Hard Mater. 28 (2010) 338–342 https://doi.org/10.1016/j.ijrmhm.2009.11.008.
[11] K. Takagi, M. Komai, T. Ide, T. Watanabe, Y. Kondo, Effects of Mo/B atomic ratio on the properties and structure of iron–molybdenum complex boride base hard alloys//, J. Jpn. Soc. Powder Powder Metall. 35 (1988) 769–774 https://doi.org/10.2497/jjspm.35.769.
[12] G. Krauss, Steels: Processing, Structure, and Performance, second ed., ASM International, 2015.
[13] S. Sheikh, R. M'Saoubi, P. Flasar, M. Schwind, T. Persson, J. Yang, L. Llanes, Fracture toughness of cemented carbides: testing method and microstructural effects, Int. J. Refract. Metals Hard Mater. 49 (2015) 153–160 https://doi.org/10.1016/j.ijrmhm.2014.08.018.
[14] R.M. German, P. Suri, S.J. Park, Review: liquid phase sintering, J. Math. Sci. 44 (2009) 1–39 2009 https://doi.org/10.1007/s10853-008-3008-0.
[15] T. Ido, T. Ando, Reaction sintering of an Fe-6 wt pct B-48 wt pct Mo alloy in the presence of liquid phases, Metal. trans. 20 (1) (1989) 18–24 https://doi.org/10.1007/BF02647490.
[16] R.M. German, P. Suri, S.J. Park, Review: liquid phase sintering, J. Mater. Sci. 44 (2009) 1–39 https://doi.org/10.1007/s10853-008-3008-0.
[17] G.A. Roberts, G. Krauss, R. Kennedy, Tool Steels, fifth ed., ASM International, Metal Park, 1998, p. 364.
[18] H. McCoy, R. Gehlbach, Influence of irradiation temperature on the creep-rupture properties of Hastelloy-N, Nucl. Technol. 11 (1) (1971) 45–60 https://doi.org/10.13182/NT71-A30901.
[19] Zh Xu, L. Jiang, J. Dong, Zh Li, X. Zhou, The effect of silicon on precipitation and decomposition behaviors of M_6C carbide in a Ni–Mo–Cr superalloy, J. Alloy. Comp. 728 (2017) 917–926 https://doi.org/10.1016/j.jallcom.2014.09.112.
[20] R. Gehlbach, H. McCoy Jr., Phase instability in hastelloy N, International Symposium on Structural Stability in Superalloys, Seven Springs, 1968, pp. 346–366.
[21] R. Warren, Microstructural development during the liquid-phase sintering of two phase alloys, with special reference to the NbC/Co system//, J. Mater. Sci. 3 (1968) 471–485 https://doi.org/10.1007/BF00549730.
[22] R. Warren, B. Johanneson, The fracture toughness of hardmetals, Int. J Refractory and Hard Mater. 2 (1984) 187–191.

[23] B. Roebuck, E.A. Almond, Deformation and fracture processes and the physical metallurgy of WC-Co hardmetals, Int. Mater. Rev. 33 (2) (1988) 90–109 https://doi.org/10.1179/095066088790324094.
[24] W.D. Schubert, H. Neumeister, G. Kinger, B. Lux, Hardness to toughness relationship of fine-grained WC-Co hardmetals, Int. J Refractory and Hard Mater. 16 (1998) 133–142 https://doi.org/10.1016/S0263-4368(98)00028-6.
[25] I. Konyashin, B. Ries, D. Hlawatschek, Y. Zhuk, A. Mazilkin, B. Straumal, F. Dorn, D. Park, Wear-resistance and hardness: are they directly related for nanostructured hard materials? Int. J. Refract. Metals Hard Mater. 49 (2015) 203–211 https://doi.org/10.1016/j.ijrmhm.2014.06.017.
[26] Z.F. Zhigang, Correlation of transverse rupture strength of WC–Co with hardness, Int. J Refractory and Hard Mater. 23 (2) (2005) 119–127 https://doi.org/10.1016/j.ijrmhm.2004.11.005.
[27] J. Jung, Sh Kang, Effect of ultra-fine powders on the microstructure of Ti(CN)–xWC–Ni cermets, Acta Mater. 52 (2004) 1379–1386 https://doi.org/10.1016/j.actamat.2003.11.021.
[28] H. Xiong, Yu Wen, X. Gan, Zh Li, L. Chai, Influence of coarse TiCN content on the morphology and mechanical properties of ultrafine TiCN-based cermets, Mater. Sci. Eng. A 682 (2017) 648–655 https://doi.org/10.1016/j.msea.2016.11.085.
[29] D. Mari, S. Bolognini, G. Feusier, T. Cutard, T. Viatte, W. Benoit, TiMoCN-based cermets Part II. Microstructure and room temperature mechanical properties, Int. J. Refract. Metals Hard Mater. 21 (2003) 47–53 https://doi.org/10.1016/S0263-4368(03)00011-8.
[30] H. Xiong, Zh Li, K. Zhou, TiC whisker reinforced ultra-fine TiC-based cermets: microstructure and mechanical properties, Ceram. Int. 42 (2016) 6858–6867 https://doi.org/10.1016/j.ceramint.2016.01.069.
[31] Ch Park, S. Nam, Sh Kang, Carbide/binder interfaces in Ti(CN)-(Ti,W)C/(Ti,W)(CN)-based cermets, J. Alloy. Comp. 657 (2016) 671–677 https://doi.org/10.1016/j.jallcom.2015.10.121.
[32] Ch Park, S. Nam, Sh Kang, Enhanced toughness of titanium carbonitride-based cermets by addition of (Ti,W)C carbides, Mater. Sci. Eng. A 649 (2016) 400–406 https://doi.org/10.1016/j.msea.2015.10.025.
[33] J. Wang, Y. Liu, J. Ye, S. Ma, J. Pang, The fabrication of multi-core structure cermets based on (Ti,W,Ta)CN and TiCN solid-solution powders, Int. J. Refract. Metals Hard Mater. 64 (2016) 294–300 https://doi.org/10.1016/j.ijrmhm.2016.09.011.
[34] S.-W. Oh, S.-Y. Ahn, K.-S. Oh, H. Lee, T.-J. Chung, Investigation into the microstructure and cutting performance of (Ti,Ta,W)(CN)–Co/Ni cermets//, Int. J. Refract. Metals Hard Mater. 53 (2015) 36–40 https://doi.org/10.1016/j.ijrmhm.2015.04.017.
[35] S. Park, Sh Kang, Toughened ultra-fine (Ti,W)(CN)–Ni cermets, Scr. Mater. 52 (2005) 129–133 https://doi.org/10.1016/j.scriptamat.2004.09.017.
[36] S. Maiti, Linear elastic fracture mechanics, Fracture Mechanics: Fundamentals and Applications, Cambridge University Press, Cambridge, 2015, pp. 6–64 https://doi.org/10.1017/CBO9781316156438.003.
[37] B.B. Straumal, A.B. Straumal, A.A. Mazilkin, K.I. Kolesnikova, B. Baretzky, I. Konyashin, B. Ries, A.M. Gusak, Pseudopartial wetting of WC/WC grain boundaries in cemented carbides, Mater. Lett. 147 (2015) 105–108 https://doi.org/10.1016/j.matlet.2015.02.029.
[38] I. Konyashin, B. Ries, B.B. Straumal, K.I. Kolesnikova, M.F. Bulatov, Contact angles of WC/WC grain boundaries with binder in cemented carbides with various carbon content, Mater. Lett. 196 (2017) 1–3 https://doi.org/10.1016/j.matlet.2017.03.001.
[39] B.B. Straumal, A.A. Mazilkin, S.G. Protasova, A.M. Gusak, M.F. Bulatov, A.B. Straumal, B. Baretzky, Grain boundary phenomena in NdFeB-based hard magnetic alloys, Rev. Adv. Mater. Sci. 38 (2014) 17–28 https://doi.org/10.1007/s10853-012-6618-5.